Vol. 74: 201–216, 2018
https://doi.org/10.3354/cr01499

CLIMATE RESEARCH
Clim Res

Published online January 29

Half-century perspectives on North American spring snowline and snow cover associations with the Pacific–North American teleconnection pattern

Thomas J. Ballinger[1,*], Robert V. Rohli[2], Michael J. Allen[3], David A. Robinson[4], Thomas W. Estilow[4]

[1]Department of Geography, Texas State University, San Marcos, TX 78666, USA
[2]Department of Oceanography and Coastal Sciences, Louisiana State University, Baton Rouge, LA 70803, USA
[3]Department of Political Science and Geography, Old Dominion University, Norfolk, VA 23529, USA
[4]Department of Geography, Rutgers, The State University of New Jersey, Piscataway, NJ 08854, USA

ABSTRACT: Spring (MAM) snow coverage across North America (NA) has significantly declined during the last half-century (1967–2016), with possible linkages to changing behaviors in large-scale atmospheric circulation. In this study, we investigated relationships between intraseasonal, sub-continental NA snow cover characteristics and the Pacific–North American (PNA) teleconnection pattern, which quantifies longwave, ridge–trough fluctuations in the 500 hPa geopotential height (GPH) field over the Northern Hemisphere. Correlation and composite techniques were applied to analyze NA spring and intra-spring snow cover extent (SCE) and snowline (SL) associations with PNA index variations. Results show the PNA pattern to be significantly correlated to interannual SL and SCE during April and climatological spring, particularly over western NA. Anomalous PNA values (i.e. exceeding ±1 SD from the index mean) particularly influence transient snow in early/mid-spring. Composites of 500 hPa GPH and low-level air temperature fields suggest that both positive and negative March PNA index anomalies are linked with expansion of western and NA-wide snow cover, while positive (negative) April PNA anomalies yield retreat (advance) to varying magnitudes across sub-continental NA. Seasonal persistence of the PNA pattern is also an important factor in determining regional snow conditions, as negative PNA values in March–April favors above-normal total spring snow coverage, while positive PNA values in these months evoke a slight retreat (advance) that is dependent on negative (positive) phase persistence through May. This study provides additional insight into mid-tropospheric circulation connections to NA springtime snow cover during an era of rapid climate and environmental change.

KEY WORDS: Snow cover extent · Snowline · Pacific–North American teleconnection pattern · North America

1. INTRODUCTION

Terrestrial snow cover has multifaceted and multi-scale physical impacts within the global climate system, underscoring the importance of identifying regional-to-hemispheric processes that drive its variability and change. Although accelerated water vapor and cloud feedbacks represent a greater source of global warming, improved understanding of the surface–atmosphere energy fluxes, including the snow–ice–albedo feedback, is of major importance for improving projections of future climate, especially at regional scales (Thackeray & Fletcher 2016).

To better quantify the role of snow on climate, an ongoing effort has been made since the late 1980s

*Corresponding author: tballinger@txstate.edu

(Robinson & Kukla 1988, Robinson 1989, Robinson et al. 1993, Brown 2000) to consolidate disparate regional collections of long-term snow cover records into a homogenized Northern Hemisphere (NH) snow database. Regional datasets became available for North America (NA) by the end of the 20th century (Frei et al. 1999, Brown et al. 2003). Studies such as those by Kunkel et al. (2007, 2009) have emphasized quality control of individual station records while assembling multidecadal snow cover datasets. Recently, long-term NH (Estilow et al. 2015) and Arctic (Brown et al. 2010) snow cover extent (SCE) databases have been developed using multiple data sources. Satellite-based products are indispensable in compiling snow datasets (Frei et al. 2012) as they have the capabilities to spatially and temporally validate interpolated snow variables obtained from station observations (Kluver et al. 2016).

The development of snow datasets has allowed for investigations of temporal trends in NH snow cover. Analyses have clearly suggested widespread, diminished spring SCE since the 1980s (e.g. Rupp et al. 2013, Comiso & Hall 2014, Kim et al. 2015, Kunkel et al. 2016, Najafi et al. 2016). Accelerated spring snow losses have been noted in recent decades (Brown & Robinson 2011), especially since 2005 across the terrestrial Arctic (Derksen et al. 2016). In addition to the observed spatial trends, a change in the timing of snowmelt has also been documented. While Peng et al. (2013) reported stability in the date of the last 5 d period of observed ephemeral snow coverage, studies have reported a tendency toward earlier spring melt onset (e.g. Foster et al. 2013, Hernández-Henríquez et al. 2015) with significant interannual variability in recent years (Wang et al. 2015). Thackeray & Fletcher (2016) acknowledged that the magnitude of the negative trend in spring NH snow cover (Derksen & Brown 2012) has exceeded the declining trend in September Arctic sea ice extent.

Although some research on NH terrestrial SCE has focused on Eurasia (e.g. Bulygina et al. 2009, Ghatak et al. 2010a, Brown & Derksen 2013, Dai & Che 2014), many regional observations have been made across NA. For example, Walsh et al. (1982) evaluated ephemeral snow cover characteristics over the contiguous US from 1949–50 to 1980–81 and found increasing variability toward the end of the record with anomalously heavy (light) snow coverage in the late 1970s (early 1980s). Leathers et al. (1993) noted a temporal increase in snowfall totals from the mid-20th century to the mid-1980s across much of the US. Knowles (2015) found an increasingly early snowmelt onset in the eastern and western US from 1950–2010, while the snow season lengthened in the Great Plains and southern Rockies. Spatiotemporal studies of regional snow coverage are critical due to associated weather and climate linkages with the strength and position of the polar jet stream (Hall et al. 2015), storm tracks (Ross & Walsh 1986), and the NA monsoon (Hawkins et al. 2002).

Some causal mechanisms for hemispheric-scale snow cover variability have been identified through comparisons with ocean–atmosphere teleconnections. Foster et al. (2013) analyzed spring Arctic Oscillation (AO) associations with the timing of NH snowmelt, and noted that a positive (negative) AO phase tends to promote earlier (later) snowmelt. Other regional work has linked the North Atlantic Oscillation (NAO) to snow cover patterns in Europe and the US (Bednorz 2004, Ghatak et al. 2010b, Henderson & Leathers 2010). The winter Pacific Decadal Oscillation (PDO) and Central Equatorial Pacific Niño 3.4 sea surface temperatures (SSTs) have also been linked to snowfall over the US Pacific Northwest and South Central Plains/Southwest regions, respectively (Kluver & Leathers 2015). Further, McCabe & Dettinger (2002) found significant, negative correlations between the western NA 1 April snowpack conditions and the preceding summer, autumn, and winter PDO, which suggests of a weakened North Pacific storm track forcing of snow along near-coastal areas stretching from Alaska to California. Relative to the PDO, the authors noted weak snowpack linkages to eastern equatorial Pacific Niño 3 regional SSTs in the aforementioned seasons.

The amplitude of the longwave ridge–trough configuration representing the Pacific–North American (PNA) teleconnection pattern has been associated with NA snow characteristics (Serreze et al. 1998, Frei & Robinson 1999, Ge et al. 2009, Abatzoglou 2011, Kluver & Leathers 2015). Ge et al. (2009) noted that the positive PNA pattern (i.e. with an enhanced western ridge–eastern trough wave train over NA) during winter influences anomalously high temperatures and low precipitation, leading to shallow snow depths in March–April near northwestern NA coastal areas, though these spatial relationships weaken over continental environments poleward of 60° N (Ballinger & Sheridan 2016). Kluver & Leathers (2015) provided regional insights on winter snowfall events exceeding 2 inches (~5 cm), noting that the PNA pattern index is negatively correlated with US Pacific Northwest, Midwest, and Northeast events where larger (smaller) snowfalls are found during negative (positive) PNA modes. Abatzoglou (2011) noted an increased incidence of late winter positive

PNA pattern occurrences since the late 1950s associated with accelerated snowpack melt over high elevation, mountainous terrain across the western US.

Research has linked diminished spring/summer snow coverage to low-to-mid-tropospheric warming and enhanced thermal ridging of atmospheric circulation, including flow reminiscent of the PNA pattern, overlying significant snow loss regions (Francis & Vavrus 2012, Tang et al. 2014). Given the physical connections between snow cover and overlying atmospheric circulation (e.g. Walsh et al. 1982, Leathers et al. 2002), there has been relatively little research holistically investigating regional and continental associations between the PNA teleconnection pattern and spring NA SCE behaviors. Here we present a half-century analysis of SCE and snowline (SL) associations with the PNA index that focuses on assessing spring and intra-spring snow characteristics by PNA phase. The purpose of this study is to enhance understanding of how oscillations and persistence in the NH 500 hPa geopotential height (GPH) field, as interpreted from behaviors of the PNA mode, relate to the 50 yr record of NA continental and sub-continental snow coverage.

2. DATA AND METHODS

2.1. Description of snow cover, PNA index, and reanalysis data

We used the NH terrestrial SCE climate data record (CDR) from the Rutgers University Global Snow Laboratory (Robinson & Estilow 2012) (http://climate.rutgers.edu/snowcover/). This dataset is composed of satellite-derived SCE measurements from multiple sources, including the Environmental Science Services Administration (ESSA), National Oceanic and Atmospheric Administration (NOAA) Polar-Orbiting Environmental Satellites (POES), NOAA Geostationary Operational Environmental Satellites (GOES), Defense Meteorological Satellite Program (DMSP) suite, Meteosat family, Geostationary Meteorological Satellites (GMS), National Aeronautics and Space Administration Aqua and Terra satellites, and Multifunctional Transport Satellites (MTSAT). The dataset has been homogenized to create a consistent CDR that includes all spring months (MAM) from 1967 to 2016 (Estilow et al. 2015). Monthly SCE is determined per grid cell based on the percentage of days within each month (using the weekly snow product) that have observable snow on the ground (grid cells ≥50% snow covered). The SCE is mapped to an 88 × 88 cell grid that overlays a polar stereographic projected map covering the entire area of the NH potentially covered with snow. Cell areas are roughly 10 700 km^2 at the Equator and approximately 41 800 km^2 at the North Pole.

From the NH SCE dataset, NA regional SCE and SL latitude time series are created for climatological spring (MAM) and its individual months. SCE is expressed as the total area of snow coverage (km^2). The SL is identified as the southernmost grid cell of snow coverage (°N) that has continuous snowpack (i.e. snow-free cells not detected) extending northward at least 5°N from that latitudinal position. We analyzed both snow variables within a regional and continental context. The SCE and SL data are initially analyzed across 3 longitudinal sectors, including Alaska (180–140° W) and Western (140–100° W) and Eastern (100–50° W) NA. The Alaska region is subsequently excluded because it registers nearly constant terrestrial snow coverage in March over the 50 yr study period and discontinuous, patchy snow cover in May due to mountainous terrain across several latitudinal zones. The Western and Eastern regions described above are separated by a black, north–south line across North America (see Fig. 1). In addition to regional analyses, SCE and SL are also calculated across NA spanning the Western and Eastern sectors from 140–50° W. The NA SL represents the southernmost, continuous snow location within the Western or Eastern region, while seasonal SL values reflect the respective 3 mo mean of this geographic position. NA SCE is calculated as the sum of the Western and Eastern region snow coverage data.

The PNA index from the NOAA Climate Prediction Center is employed in this study (www.cpc.ncep.noaa.gov/products/precip/CWlink/pna/pna.shtml). This index is created by applying a rotated principal component (RPC) technique (Barnston & Livezey 1987) to the monthly standardized 500 hPa GPH anomalies poleward of 20° N. The GPH data are standardized by their 1950–2000 monthly means and standard deviations (SDs). The PNA index represents the time series resulting from the second RPC identified within the 500 hPa GPH anomalies. Monthly (March, April, and May) and spring PNA time series are analyzed with respect to the NA snow cover data.

The first generation NCEP/NCAR Reanalysis (Kalnay et al. 1996) 500 hPa GPH and 850 hPa air temperature data are aggregated accordingly to the monthly and seasonal time steps. The data, analyzed at their native 2.5° × 2.5° latitude–longitude resolution, are selected to examine the NA upper-level

atmospheric circulation and low-level thermal regimes affiliated with PNA phases, and are subsequently associated with snow characteristics as described in the Methods section. The 850 hPa layer temperatures are analyzed in lieu of near-surface fields (i.e. 925 or 1000 hPa levels) to capture high elevation surface temperatures in a standard lapse atmosphere more accurately over the complex Western region terrain. The NCEP/NCAR reanalysis data are obtained from the NOAA/Earth System Research Laboratory Physical Sciences Division (www.esrl.noaa.gov/psd/data/gridded/data.ncep.reanalysis.html).

2.2. Methods

Relationships between NA SCE and SL and the PNA pattern are evaluated through various statistical procedures. Descriptive statistics, including means and SDs, and linear trends from least squares regression, are utilized to identify the climatological monthly and spring seasonal snow cover and PNA characteristics across the regions. To gain additional understanding of NA mid-tropospheric flow behaviors connected to PNA pattern and snow cover variations, we also assess regional spatial patterns of the polar jet stream. Utilizing a similar technique to that of Ballinger et al. (2014), the southernmost latitude (°N) of the monthly/seasonal polar jet, represented by the 5600 m isohypse, is identified within the 500 hPa GPH field found above each of the 3 longitudinal sectors. This particular contour is generally located within the strongest spring 500 hPa GPH gradient, and therefore is embedded amidst the fastest mean mid-tropospheric winds observed during the season of interest (Francis & Skific 2015, Francis & Vavrus 2015).

Temporal associations between snow variables and the PNA pattern are evaluated through correlation analyses. A Shapiro-Wilk test is initially applied to all snow and PNA time series to assess normality characteristics of the data distributions. Some of the SL latitude time series exhibit positive skewness, which prompted application of the non-parametric Spearman rank (r_s) correlation technique to analyze monthly and seasonal snow–PNA pattern associations since 1967. Scatter plots are also used to explore the degree of association amongst the primary variables. Prior to calculating the correlation coefficients, linear trends are removed from the respective time series to emphasize interannual snow–PNA pattern relationships. Statistical significance in the period-long trend and correlation analyses is determined by the 95% confidence level ($p \leq 0.05$) using a Student's 2-tailed *t*-test. For analyses conducted over abbreviated time periods, significance is not assessed via *t*-test or additional statistical methods. Motivations to withhold testing differences between small samples ($n < 30$ yr) follow recent literature suggesting that it is only within the last ~15–20 yr that accelerated NH snow and ice loss signals associated with Arctic amplification have become distinguishable from climate system noise (Overland 2016, Overland et al. 2016).

Composite analyses are conducted to isolate the common, regional snow responses to the PNA phases. Average monthly and seasonal SL and SCE conditions are evaluated by 4 criteria, including PNA positive (+) years, extreme PNA+ (i.e. with values of at least +1, abbreviated as such), PNA negative (−) years, and extreme PNA− (i.e. values of −1 or less, abbreviated as such). All snow values are shown as anomalies with respect to the 1981–2010 normal period, which is currently used in historical snow analyses conducted by the Rutgers Global Snow Laboratory and NOAA National Centers for Environmental Information. Additional insight into SL and SCE associations with upper-level atmospheric circulation is facilitated through monthly and seasonal composite 500 hPa GPH anomaly plots during extreme PNA phases. These synoptic maps are presented with respect to the 1981–2010 mean GPH values. Supplemental 850 hPa air temperature composites, which use raw data, are presented to indicate areas of warm/cold air that are subsequently advected by the circulation patterns.

Finally, the role of intraseasonal PNA phase distributions on the seasonal SL and SCE characteristics is explored. Composite mean SL and SCE values are calculated based on the March, April, and May PNA phase sequence observed during each spring. Specifically, 8 different PNA distributions are possible: +++, ++−, −++, +−+, −+−, −−+, +−−, and −−−. For example, a spring when the PNA+ phase occurs during both March and April, but a PNA− phase transpires during May is classified as PNA++−; SL and SCE data are subsequently averaged for every spring that exhibits this particular PNA distribution. Spring snow composites by PNA distribution are shown with respect to the 1981–2010 mean seasonal values. For all PNA distribution cases, seasonal 500 hPa GPH composite anomaly maps (relative to the 1981–2010 mean) are generated to identify the synoptic circulation features associated with seasonal SL and SCE.

3. RESULTS AND DISCUSSION

3.1. Overview analysis of the SL and SCE data

Boreal spring represents an especially active period of ephemeral snow cover ablation across the high and middle latitudes of NA (Brown & Robinson 2011, Foster et al. 2013). Climatological characteristics, including the mean position of the SL and the standard deviation of the latitude demarcating the SL, along with the SCE mean and standard deviation, are shown in Table 1. The half-century SL and SCE time series are also presented in Fig. S1 in the Supplement at www.int-res.com/articles/suppl/c074p201_supp.pdf. Of note, SL variability is much greater in the West than in the East for all spring months, and the SL position significantly retreats poleward over time in the West for all spring months and for NA in March and April. Similarly, the SCE mean and variability characteristics are greater over the West than the East in all spring months, and the SCE area is decreasing over time in all regions (Table 1).

Table 1. Descriptive statistics and trends of snow cover extent (SCE) and the snowline (SL), for the 1967–2016 study period, by region; W: Western (140–100° W); E: Eastern (100–50° W); NA: North America (140–50° W). SL mean is indicated in decimal coordinates (° N, ° W), while the SL standard deviation (SD) and trend values reflect latitude variability and change. Trends are displayed as decadal values (SL = ° N decade^{-1} and SCE = ×10^5 km^2 decade^{-1}) with significant regression coefficients ($p \leq 0.05$) shown in **bold**. Corresponding time series are presented in Fig. S1 in the Supplement at www.int-res.com/articles/suppl/c074p201_supp.pdf

Region	SL (° N)			SCE (10^5 km^2)		
	Mean	SD	Trend	Mean	SD	Trend
March						
W	41.79, 110.90	4.25	**+1.00**	62.24	5.08	−0.53
E	41.95, 77.49	1.62	+0.20	57.78	3.70	−0.34
NA	40.11, 93.18	2.52	**+0.80**	120.03	7.54	−0.87
April						
W	48.26, 117.17	4.80	**+1.10**	49.03	5.38	−0.99
E	45.75, 71.50	1.56	+0.10	46.10	4.58	−0.34
NA	44.77, 82.60	2.60	**+0.50**	95.13	9.05	−1.33
May						
W	54.89, 125.42	2.68	**+0.80**	31.15	4.57	−1.44
E	50.89, 66.78	1.53	+0.10	29.62	3.51	−0.54
NA	50.82, 70.79	1.41	+0.10	60.78	7.26	**−1.98**
MAM						
W	48.32, 117.83	2.89	**+1.00**	47.47	3.91	**−0.99**
E	46.20, 71.92	1.11	+0.10	44.50	3.13	−0.41
NA	45.23, 94.88	1.45	+0.50	91.98	6.35	**−1.40**

While regional SL trends are positive (indicating retreat), the Western and NA change signals are typically of greater magnitude and statistically significant compared to the monthly trends of the Eastern region (Table 1). As climatological spring proceeds from March to May, retreat of the mean SL is rather abrupt in the Western region, shifting in a southeast to northwest fashion along the Rocky Mountains, while the Eastern SL retreats poleward more slowly from the northeastern US in March toward the southwestern edge of Labrador in May (Fig. 1). Spatial coverage characteristics of West and East monthly SCE are largely similar. For instance, average SCE declines by 36% from April to May in both regions. However, SCE losses are clearly accelerated toward the conclusion of spring, that is from April to May versus March to April.

PNA and polar jet climatologies are detailed in Table 2 and the respective time series are shown in Fig. S2. Slightly positive mean PNA values (< +0.20) are found in March, April, and spring-wide, while the climatological polar jet position shifts toward the northwest in a fashion similar to the Western SL through the spring months. Since 1967, the PNA index is shown to increase slightly at +0.06 standardized PNA values decade^{-1} in March and April and decrease at −0.15 standardized PNA values decade^{-1} in May, although these trends are not statistically significant. Within the NH upper-level flow described by the PNA pattern, pronounced multidecadal trends are observed in the position of the polar jet latitude over NA. West sector trends are especially notable as shown by strong poleward shifts in jet latitude (≥+0.75° N decade^{-1}) during March and April. By extrapolating these trends over the study era, a northward shift in the climatological jet winds of at least +3.75° N (or >400 km) can be inferred, which is of similar magnitude to the Western SL trend (see Table 1). Spatial changes in the polar jet positioning may reflect a warm-season reduction in the strength of zonal winds connected to the increasingly early and rapid retreat of terrestrial snow cover (Tang et al. 2014, Coumou et al. 2015).

3.2. Correlations between SL/SCE and PNA pattern

Links between the PNA mode and the snow data are initially explored through detrended correlation analyses (Table 3). A comparative assessment shows that the original, unadjusted PNA index and snow variables yield similar magnitude correlations as the detrended datasets (not shown), suggesting that peri-

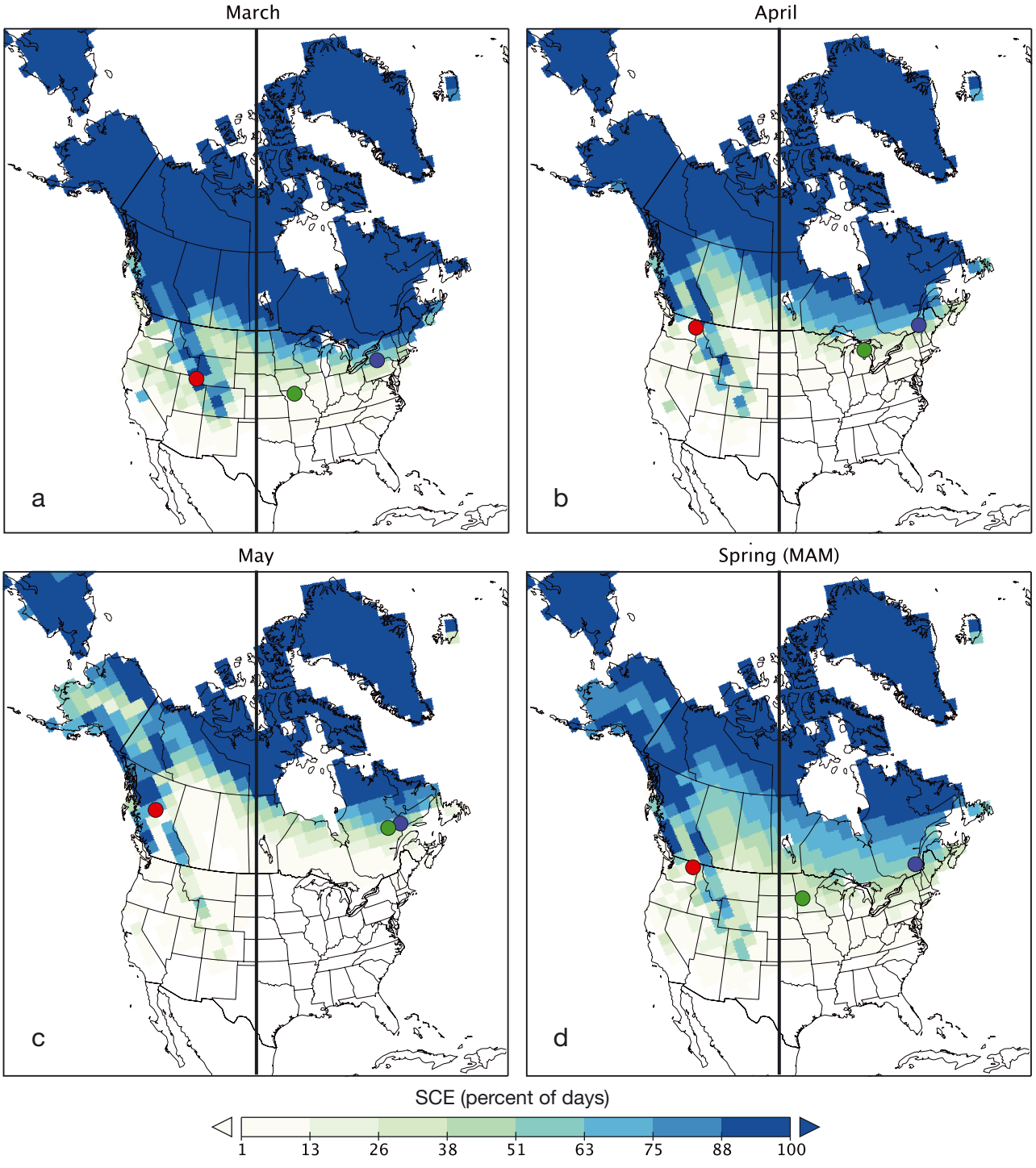

Fig. 1. (a–c) Monthly and (d) spring snow cover extent (SCE) climatology, 1967–2016. Mean snowline (SL) positions are indicated in each map for the Western (red dot), Eastern (blue dot), and North American (green dot) regions. The black line delineates 100° W, which is the longitudinal boundary selected to separate the Western and Eastern regions. Additional SCE and SL climatological details are presented in Table 1

ods of interannual co-variability between snow and the PNA pattern influence the temporal relationships in a similar manner as the underlying trend. The sign of coefficients is consistent by snow variable as primarily positive correlations are found between SL latitudes and PNA mode (i.e. SL retreat [advance] is connected to increasing [decreasing] PNA values and amplified [reduced] meridionality in the mid-tropos-

Table 2. Descriptive statistics and trends of the Pacific–North American (PNA) index and polar jet stream (PJS) by region for the 1967–2016 study period. The mean latitude of the polar jet is indicated in decimal coordinates (°N, °W), while the jet SD and trend values indicate latitude variability and change metrics. Trends are displayed as decadal values (PNA = standardized PNA values decade^{-1}, and polar jet = ° N decade^{-1}). Significant regression coefficients ($p \leq 0.05$) are presented in **bold**. Region abbreviations as in Table 1. Corresponding time series are presented in Fig. S2 in the Supplement at www.int-res.com/articles/suppl/c074p201_supp.pdf

Region	Mean	SD	Trend
March			
PNA	0.17	0.95	+0.06
PJS			
W	37.36, 117.76	2.34	**+0.82**
E	36.53, 77.36	1.92	+0.35
NA	36.03, 93.57	1.86	**+0.45**
April			
PNA	0.09	1.04	+0.06
PJS			
W	40.01, 123.76	2.56	**+0.75**
E	38.99, 72.53	1.85	**+0.52**
NA	38.53, 86.72	1.97	**+0.70**
May			
PNA	−0.08	1.00	−0.15
PJS			
W	45.35, 130.93	2.94	+0.54
E	44.90, 64.11	2.71	**+0.60**
NA	43.75, 91.73	2.38	+0.33
MAM			
PNA	0.06	0.69	−0.01
PJS			
W	40.91, 124.15	1.86	**+0.70**
E	40.14, 71.33	1.38	**+0.49**
NA	39.44, 90.67	1.33	**+0.49**

Table 3. Detrended Spearman's correlation coefficients between regional snowline (SL) and snow cover extent (SCE) and the overlapping detrended Pacific–North American (PNA) index values. Significant coefficients ($p \leq 0.05$) are indicated in **bold**. Time series overplots are presented in Figs. 2 & 3. Region abbreviations as in Table 1

Region	SL	SCE
March		
W	+0.06	−0.28
E	−0.12	−0.12
NA	−0.24	−0.24
April		
W	**+0.35**	**−0.43**
E	**+0.30**	**−0.42**
NA	**+0.33**	**−0.49**
May		
W	−0.03	−0.08
E	+0.04	−0.05
NA	+0.04	−0.07
MAM		
W	**+0.30**	**−0.40**
E	+0.21	**−0.40**
NA	**+0.30**	**−0.42**

pheric circulation over western NA). Likewise, negative correlations are observed between SCE and the PNA index (i.e. increasing SCE is associated with both decreasing PNA values and meridionality of mid-tropospheric circulation over Western NA and vice versa). These relationships are particularly noteworthy in April and for spring, when statistically significant relationships are found between SL and SCE conditions and the detrended PNA index (with the exception of the Eastern region in MAM). By contrast, March and May do not show statistically significant correlations. Poleward shifts in the SL across Western and Eastern regions and NA as a whole are generally associated with increasing PNA index values during April, with correlation coefficients ranging from +0.30 to +0.35 ($p \leq 0.05$; see Fig. S3a). Statistically significant anticorrelations of stronger magnitude between April and MAM SCE and the PNA index are roughly −0.40 in the Western and Eastern domains and peak at $r_s = -0.49$ ($p \leq 0.05$) across NA (see Fig. S3b). This set of results suggests that spring continental snow coverage, especially during April, is strongly connected to the PNA pattern.

To gain further insight into the temporal associations described previously, time series of the snow datasets and PNA index are analyzed. To aid visual interpretation, the detrended PNA indices are normalized to the same long-term mean and standard deviation as the NA monthly and seasonal SL (Fig. 2) and SCE (Fig. 3), respectively. Although the late 1970s to late 1980s period corresponds to anomalously large maximum snow depths across both NA and Eurasia (Robinson & Frei 2000), a few years (1976, 1980, and 1987) are characterized by anomalous retreats across all 3 regions corresponding to high/positive PNA values (Fig. 2b). Relationships during May also show some in-phase tendencies over this era of the snow record (Fig. 2c). Years of in-phase SL–PNA coupling are also apparent over this most recent decade (2007–2016) in the March, April, and MAM time series (Fig. 2a,b,d). This is especially the case during 2010 when positive retreat anomalies across all 3 regions coincided with an above-normal PNA index, including a Western SL that exhibited a record displacement of nearly +7° N from its 1967–2016 mean position (Fig. 2b).

Negative SCE associations with the PNA pattern are apparent in the late 1970s to late 1980s (Fig. 3). For example, April detrended time series show particularly low SCE during positive PNA anomalies in 1984 and 1987. Substantial, positive SCE anomalies also overlap with negative PNA values from the 2000s onward, especially in 2011 and 2013 in the

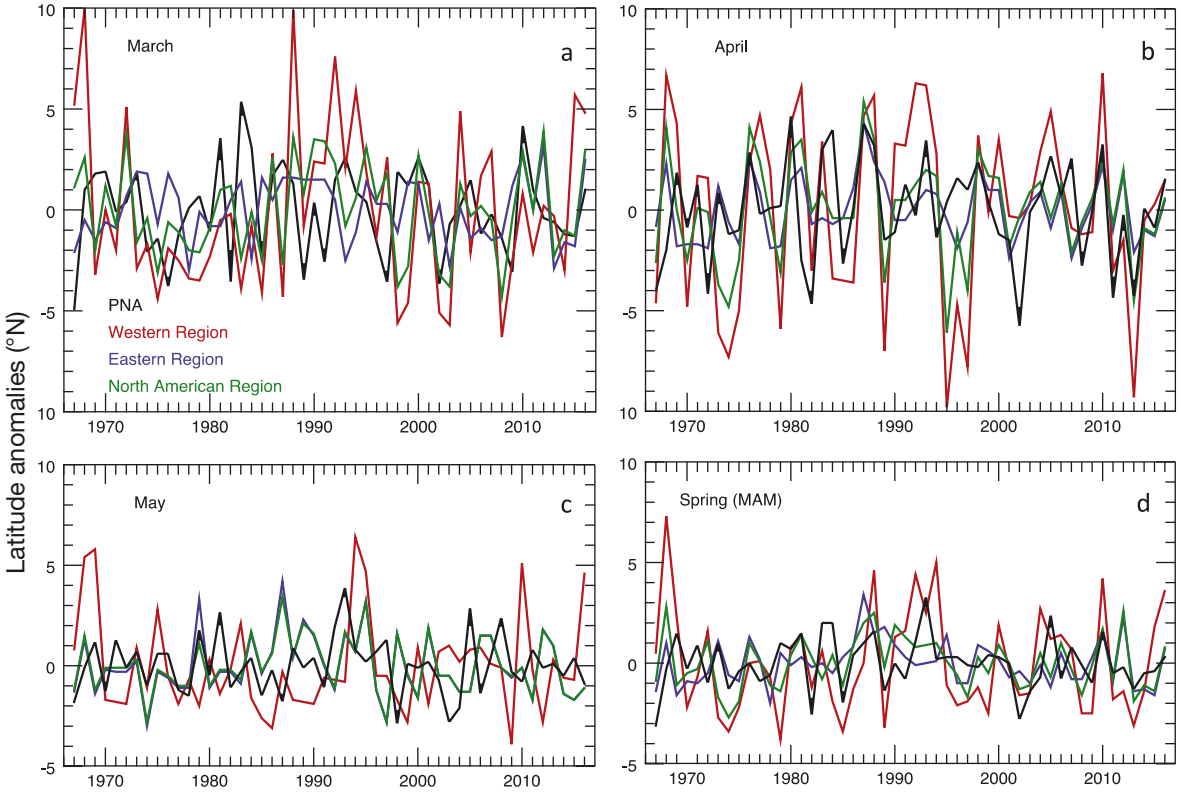

Fig. 2. Detrended anomalies of (a–c) monthly and (d) spring snowline (SL) latitudes and Pacific–North American (PNA) index values. Each PNA time series has been normalized to the respective North American region SL data. Corresponding detrended Spearman rank correlations between the PNA pattern and SL latitudes are listed in Table 3

West and over NA (Fig. 3b). With some exceptions (e.g. March SCE–PNA in 1983, May SCE–PNA in 1998), extreme PNA mode years typically coincide with strong terrestrial snow cover responses.

3.3. SL/SCE composites by PNA phase

Building upon the correlation results in the previous section, SL and SCE composite analyses are conducted by phase and extremes of the PNA pattern (Figs. 4 & 5). SL observations appear strongly influenced by the magnitude and PNA mode occurrence within spring. For instance, PNA+ mode elicits a relatively weak SL response across all spring months, but PNA+1 during March favors expansion of the SL as continuous snowpack extends anomalously southward almost 2° across the Western sector and 1° over NA longitudes (Fig. 4a), lying at 40.51° N, 109.89° W (northeast Utah) and 46.12° N, 95.32° W (west-central Minnesota), respectively. In contrast, PNA+1 composites in April yield a typical SL that recedes >2° poleward in the West and >1° northward across NA compared to respective climatological latitudes (Fig. 4b). PNA– conditions consistently coincide with negative (i.e. equatorward) SL departures. During March, PNA– elicits a stronger SL response in the West and NA regions compared to snow values linked to PNA–1 (Fig. 4a), which could be related to slight differences in the positioning of the North Pacific High or Pacific storm track by magnitude of the PNA pattern. However, during April and MAM, extreme PNA–1 yields stronger responses (versus PNA– composites), especially across the West, as areas of continuous snowpack stretch 2–3° south of their climatological mean latitudes.

Some parallels emerge in the intraseasonal relationships between the PNA pattern values, SL, and SCE. For instance, PNA+ has little impact on either SL or SCE across spring months, but PNA+1 is linked to anomalous SL retreat and SCE loss in April, particularly over the West and NA, respectively (Figs. 4b & 5b). PNA– consistently yields SL advance and overall above-average SCE in Western, Eastern, and NA longitudes in March, April, and across spring (Figs. 4a,b,d & 5a,b,d, respectively). Negative PNA values and extremes tend to yield similar SCE anomalies during March (Fig. 5a). The PNA–1 occurrences

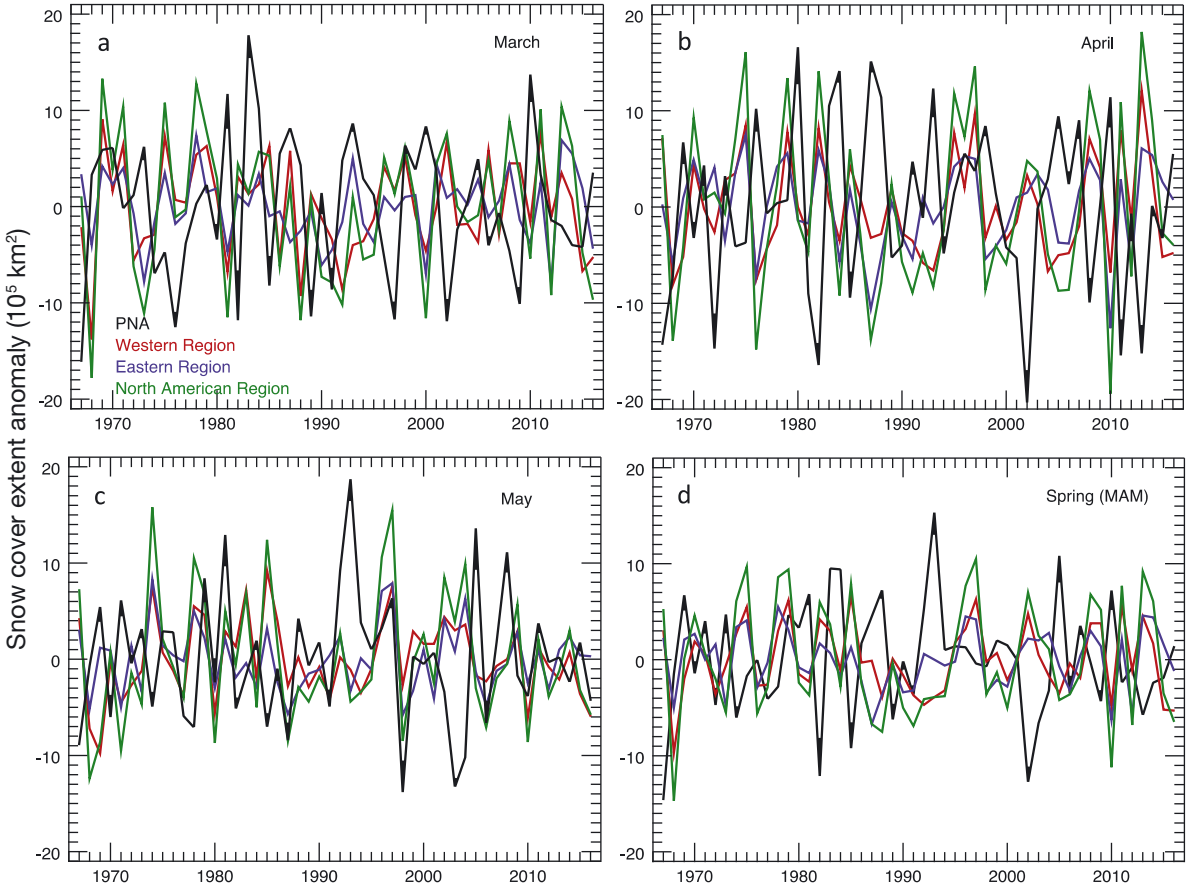

Fig. 3. Detrended anomalies of (a–c) monthly and (d) spring snow cover extent (SCE) and the Pacific–North American (PNA) index values. Each PNA time series has been normalized to the respective North American region SCE data. Corresponding detrended Spearman rank correlations between the PNA pattern and SCE are listed in Table 3

contribute to a more southward extending SL and larger SCE (versus PNA–) during April and MAM (Figs. 4b,d & 5b,d, respectively), though the strong springtime SCE response appears substantially influenced by the mid-spring signal.

Figs. 4 & 5 indicate that PNA extremes (i.e. values exceeding –1 and +1) are strongly linked to SL and SCE behaviors. Synoptic patterns affiliated with PNA extremes (listed in Table 4) are explored through 500 hPa GPH composite anomalies to better understand the role of mid-tropospheric circulation on the SL and SCE anomalies. The composite map of March PNA+1 months, when there is a prevalence of SL advance and above-normal SCE within Western longitudes, reveals a negative GPH anomaly over the Bering Sea, and upper-level, high pressure stretching eastward across Hudson Bay. The dipole pattern generates southerly flow that transports cold moist air from the Northeast Pacific Ocean onshore that becomes sub-freezing once intercepted and lifted by the Pacific Coast Range (Fig. S4), if not before. Upon condensing, this process leads to snow deposition that builds the Western snowpack (Fig. 6a). March PNA–1 also coincides with above-average snow, but is driven by a noticeably different synoptic pattern. Specifically, March PNA–1 is characterized by anomalously positive GPH values in the North Pacific Ocean and anomalously negative GPH values over most of north-central Canada. This GPH dipole creates a northerly wind regime over the Western region, allowing snow to be deposited or sustained at anomalously low latitudes by advection of below-freezing, high-latitude air (Fig. 6b and Fig. S4).

April mid-tropospheric patterns associated with PNA extremes show similarities to the March composites, but much different snowpack characteristics result. April PNA+ coincides with a strong anticyclone extending from Hudson Bay westward to Great Slave Lake and an anomalous low pressure trough that drops across the North Pacific Ocean and Gulf of Alaska. This dipole GPH pattern works in tandem to advect above-freezing, low-level air

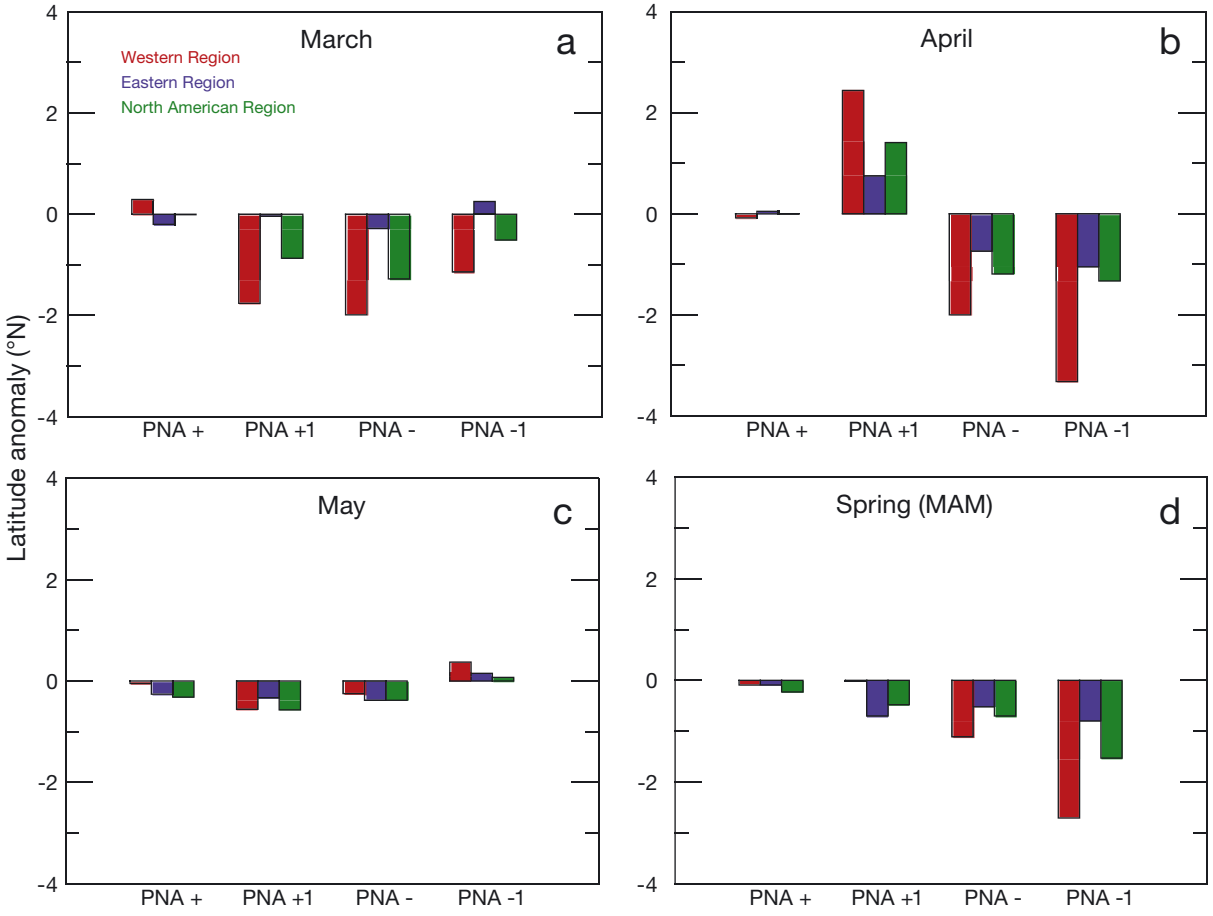

Fig. 4. Composites of (a–c) monthly and (d) spring snowline (SL) anomalies, with respect to their mean 1981–2010 SL latitudes, by Pacific–North American (PNA) phase and extremes (i.e. PNA+1 indicates values ≥+1, while PNA–1 denotes values ≤–1)

from the North Pacific onto the continent to ablate the Western SCE (Fig. S4), thereby causing the SL to shift poleward (Fig. 6c). Similarly, a low-level, southerly wind regime exists across the West in March during PNA+ conditions. In these cases, however, below-freezing 850 hPa air permeates the North Pacific (see Fig. S4), and the prevailing circulation patterns transport the cold, maritime air inland to increase SCE. Comparatively, April PNA– extremes generate stronger SL response anomaly (Fig. 4b) than March PNA– extremes (Fig. 4a) as a region of southeastward trending positive GPH anomalies stretches from the Bering Sea across the Gulf of Alaska and couples with a broad negative GPH region over Canada to direct cold, moisture-laden air from the Pacific Ocean along the NA Cordillera region (see Fig. 6d and Fig. S4). The greater April PNA– versus March PNA– positive snow anomalies could be a product of a more saturated air mass as temperatures warm through spring. Weak height gradients during May seem to play relatively little role in snow accumulation or ablation (Fig. 6e,f). The springtime 500 hPa GPH anomalies display relatively similar spatial patterns to the flow observed during the March and April PNA extreme years (Fig. 6g,h). However, a stronger snow response, manifested through negative (i.e. southward-displaced) SL and positive SCE anomalies, occurs during the PNA– versus PNA+ extreme springs (compare Figs. 4d & 5d).

3.4. SL/SCE by PNA distribution

Composite analyses in Section 3.3 reveal pronounced intraseasonal linkages between March–April snow characteristics and the temporally overlapping phase of the PNA index. The role of the monthly PNA distribution during spring on the overall spring snow observations is investigated further here. Table 5 displays SL and SCE composites by the 3 mo distribution of the PNA index. The role of the

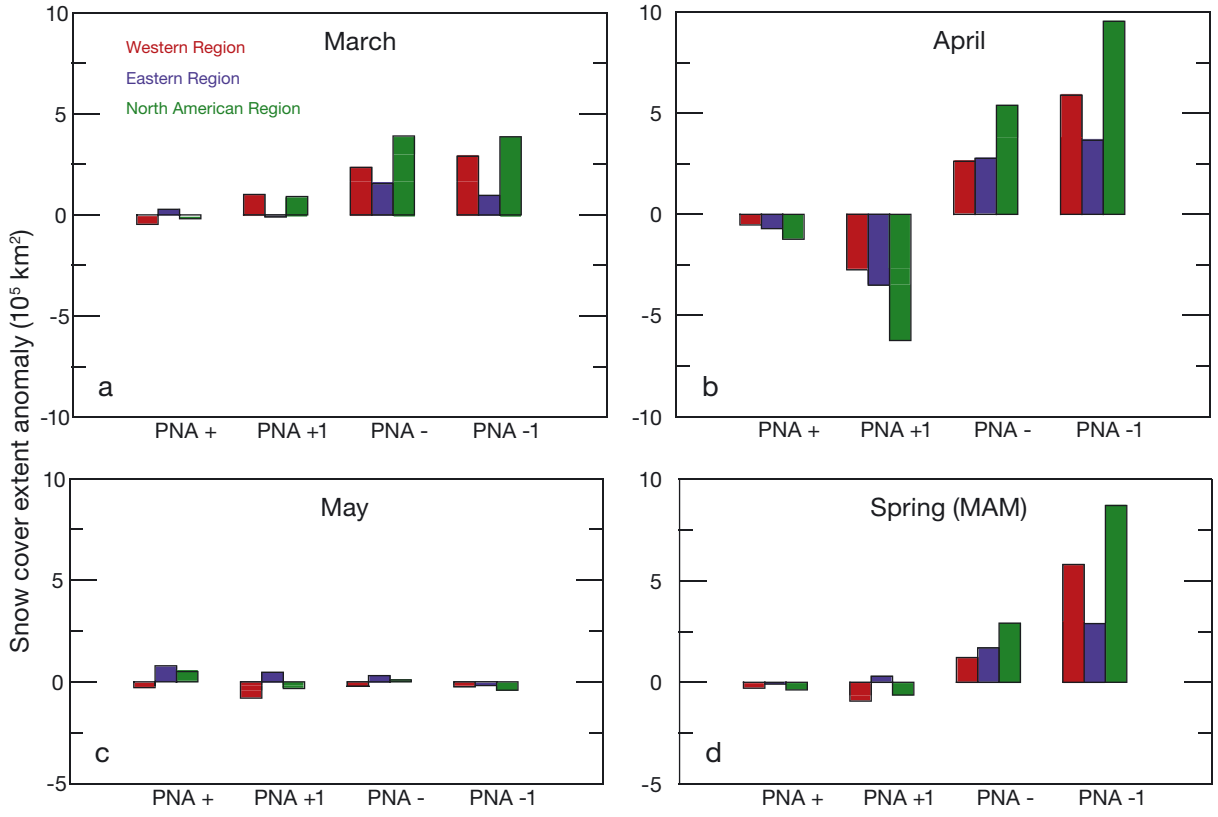

Fig. 5. Composites of (a–c) monthly and (d) spring snow cover extent (SCE) anomalies, with respect to their mean 1981–2010 SCE, by Pacific–North American (PNA) phase and extremes (i.e. PNA+1 indicates values ≥+1, while PNA–1 denotes values ≤–1)

Table 4. Extreme monthly and seasonal Pacific–North American (PNA) index values of ≥+1 and ≤–1 listed in order from strongest to weakest magnitude anomalies (1967–2016). The number of cases comprising each composite map in Fig. 6 is provided in parentheses

PNA+1	PNA–1
March	
(n = 7)	(n = 7)
1983, 2010, 1984, 2000,	1967, 1976, 1982, 1989,
1993, 1987, 1998	1997, 2002, 2009
April	
(n = 11)	(n = 8)
1980, 1987, 1984, 1993,	2002, 1982, 1972, 1967,
2010, 1988, 2005, 1983,	2011, 2013, 1985, 1981
2007, 1976, 1998	
May	
(n = 8)	(n = 7)
1993, 1981, 2005, 1979,	1998, 2004, 2006, 1987,
2008, 1992, 1971, 1969	2016, 1985, 1967
MAM	
(n = 4)	(n =4)
1993, 2005, 1983, 1984	1967, 2002, 1982, 1985

early season persistence in PNA phase, characterized by consecutive months of common sign, appears of utmost importance in dictating the spring SL or SCE anomalies. For instance, PNA++– (e.g. both March and April PNA values are positive, while May values are negative) is linked to a northward SL retreat of nearly half of a degree latitude (approximately 55 km), and at least 100 000 km^2 less SCE from average over Western and Eastern NA. This distribution pattern has been somewhat common in the last decade (2007–2016), occurring in 4/10 springs coincident with anomalous (sub)continental snow losses (not shown). Though PNA––+ is relatively uncommon (n = 2), the sequence yields a dramatic equatorward advance of the SL and above-normal SCE, while its more common PNA––– counterpart (n = 8) favors positive SCE anomalies of comparatively lower magnitude. It is interesting to note that spring-wide PNA persistence (e.g. PNA+++) appears to dampen the snow response, producing negative SL anomalies (especially in the Western region) and slight positive SCE anomalies in both the Eastern and Western domains.

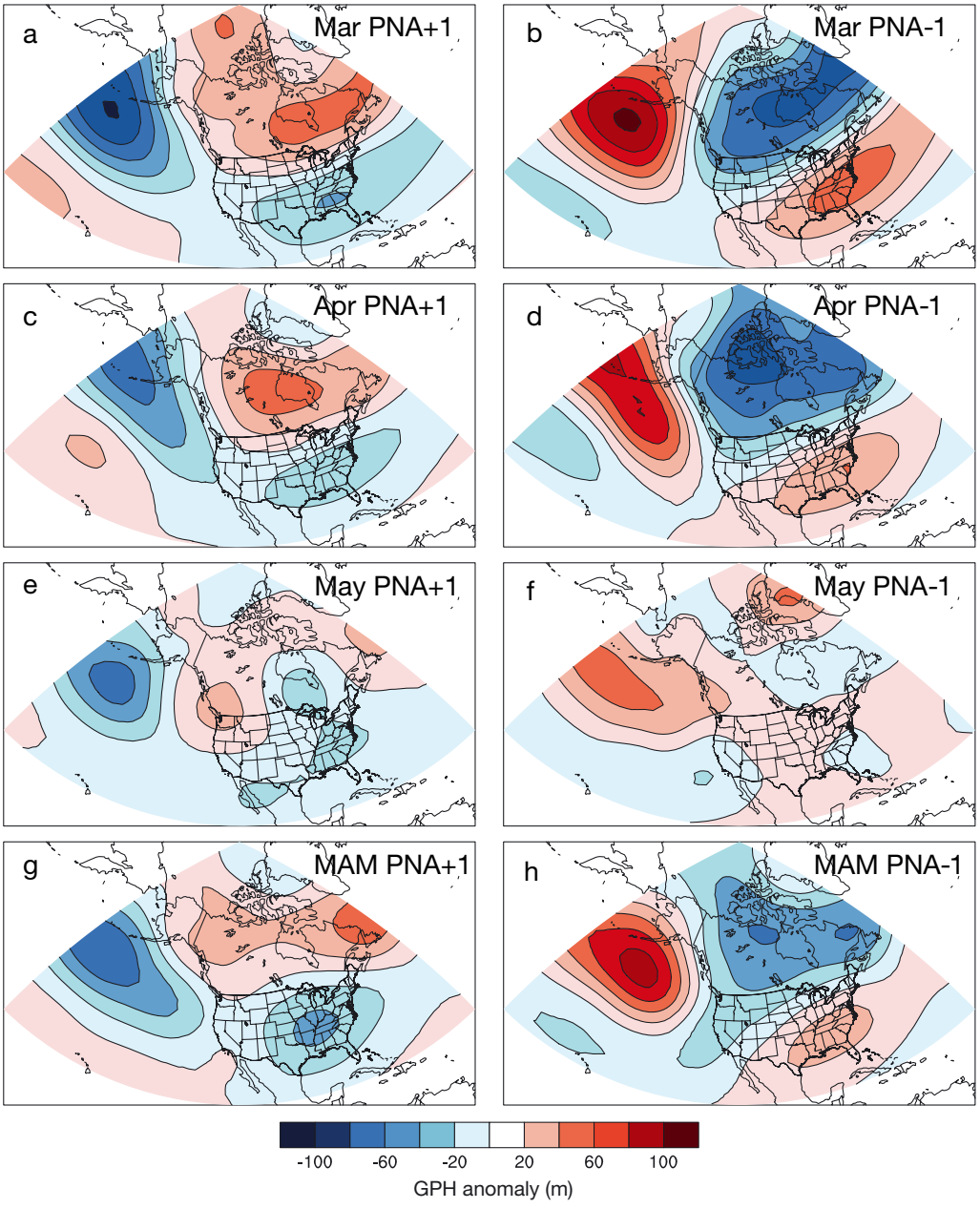

Fig. 6. Composite (a–f) monthly and (g,h) spring 500 hPa geopotential height (GPH) anomalies (from the 1981–2010 mean) during Pacific–North American (PNA)+1 and PNA–1 years, which are listed in Table 4

Mid-tropospheric GPH anomaly maps based on the intraseasonal PNA distribution are presented in Fig. 7. PNA+++ is associated with positive GPH anomalies shifted poleward that advect frigid, Arctic air southward and allow more snow across lower latitudes (Fig. 7a). By contrast, March–April persistence in the PNA positive phase (e.g. PNA++–, Fig. 7b) coincides with a broad anticyclonic anomaly centered just south of Hudson Bay that ushers warm, moist air off the US east coast and maritime Canada onshore to yield Eastern snow loss. Coupled with continental high pressure, a trough over southwest Alaska creates a slight dipole pattern that transports warm air onto Western NA and promotes snowmelt. Negative March–April phase persistence, such as PNA––+ (Fig. 7f) and PNA––– (Fig. 7h), tends to coincide with positive GPH anomalies over the North Pacific Ocean and negative GPH anomalies over continental NA. Spatial shifts in this height dipole appear to impact the regional snow conditions. The

Table 5. Composite values of snowline (SL) latitudes (°N; columns 4–6), and snow cover extent (SCE, $\times 10^5$ km^2; columns 7–9) by Pacific–North American (PNA) phase distribution during all spring seasons, 1967–2016. Eight PNA distributions are possible (+++, ++−, −++, +−+, −+−, −−+, +−−, and −−−). For example, PNA++− describes a spring when the PNA+ phase occurs during both March and April, but a PNA− phase transpires during May. PNA mean values by distribution are shown in column 3. Region abbreviations as in Table 1

Distribution	Cases (n)	PNA	SL_W	SL_E	SL_{NA}	SCE_W	SCE_E	SCE_{NA}
+++	9	+0.89	−1.23	−0.36	-0.90	+0.43	+0.36	+0.80
++−	11	+0.29	+0.51	+0.46	+0.41	−1.03	−1.19	−2.22
−++	3	+0.10	−2.09	−0.56	−0.94	+2.86	+2.72	+5.58
+−+	7	+0.13	+1.74	−0.22	+0.52	−1.92	+0.04	−1.88
−+−	6	−0.28	+0.05	−0.39	+0.02	−0.42	+0.46	+0.04
−−+	2	−0.06	−2.93	−1.13	−2.22	+5.09	+4.28	+9.37
+−−	4	−0.12	−1.02	−0.90	−0.62	+1.03	+1.79	+2.82
−−−	8	−0.90	−2.35	−0.59	−1.58	+2.62	+2.40	+5.02

GPH anomaly gradient is particularly strong during PNA−−+ and favors a northerly, geostrophic wind flow along the Pacific Coast Ranges that contributes to anomalous Western snow accumulation. At the same time, above-normal snow coverage is also found in the East region as cold, maritime air is advected onto the continent from the North Atlantic by positive GPH anomalies extending northeastward across Baffin Bay (Fig. 7f). As the aforementioned GPH anomalies shift apart in a seaward manner and their respective centers weaken (Fig. 7h), the strength of northerly winds over the continent tends to diminish, although the winds still influence anomalously equatorward snow cover across Eastern and Western NA.

4. CONCLUSIONS

A detailed intra-spring analysis of the PNA teleconnection is undertaken to gain insight into the role of synoptic circulation variability and extremes on NA SL and SCE conditions within a time of year characterized by active, yet changing terrestrial snow melt patterns (Foster et al. 2008). Analyses targeted at understanding the sub-continental snow cover response to atmospheric circulation within spring are critical, as new evidence suggests that terrestrial snow loss anomalies during this period tend to coincide with summers of enhanced jet stream amplitude and increased incidence of extreme weather conditions over North America (Vavrus et al. 2017). Over the 50 yr SCE CDR, interannual associations, identified through detrended monthly and seasonal correlation analyses, are found between the April and MAM PNA indices and SL/SCE. Strong co-variability is apparent in the respective time series from the mid-1970s to mid-1980s and since the mid-2000s. The former (latter) period has been recognized for above (below) normal spring NH snow conditions (Robinson & Frei 2000, Kunkel et al. 2016). Composite analyses of snow variables by PNA phases suggest that extreme PNA values, particularly ≤−1 standard deviation, result in an increase in regional snow coverage over the NA middle and high latitudes.

At the sub-seasonal scale, March and April snow cover anomalies by PNA extremes differ considerably despite upper-level flow similarities. This reflects a tendency across high NA latitudes for warm and cold extremes to occur with similar synoptic circulation features (Cassano et al. 2015). Cold and moist southerly flow in March is linked to southward SL advance and more abundant SCE, likely through accumulation of snow, but southerly winds and energy advection tend to increase local air temperatures above the freezing mark to elicit the opposite response (i.e. ablation of terrestrial snow) during April (Mioduszewski et al. 2015). The frequent presence of above-freezing, moist lower tropospheric air in April may prompt more rain-on-snow events (Cohen et al. 2015). Downward sensible and latent (i.e. condensation) heat flux into the snowpack through the spring months also promotes melt, particularly within the Arctic (Pohl et al. 2006). Spring 500 hPa GPH composite maps exhibit similar circulation patterns as March and April, but stronger absolute SL and SCE contrasts are found when comparing extreme PNA phases. When both March and April exhibit a positive (negative) PNA phase, spring snow tends to decrease (increase). Spring-wide PNA persistence (of either phase) favors the advancement of snow over NA, though snow coverage is particularly extensive during spring months characterized by a negative PNA phase.

Previous work has indicated that the PNA often strengthens and decays (exhibiting a 'lifecycle') during roughly a 2 wk period (Feldstein 2000), though quite often the monthly-averaged index represents persistent patterns of sub-monthly ridging and troughing (Vega et al. 1995). Future research will delve further into the (bi)weekly linkages between PNA phase and NA snow coverage. Additional research building upon this work will also investigate

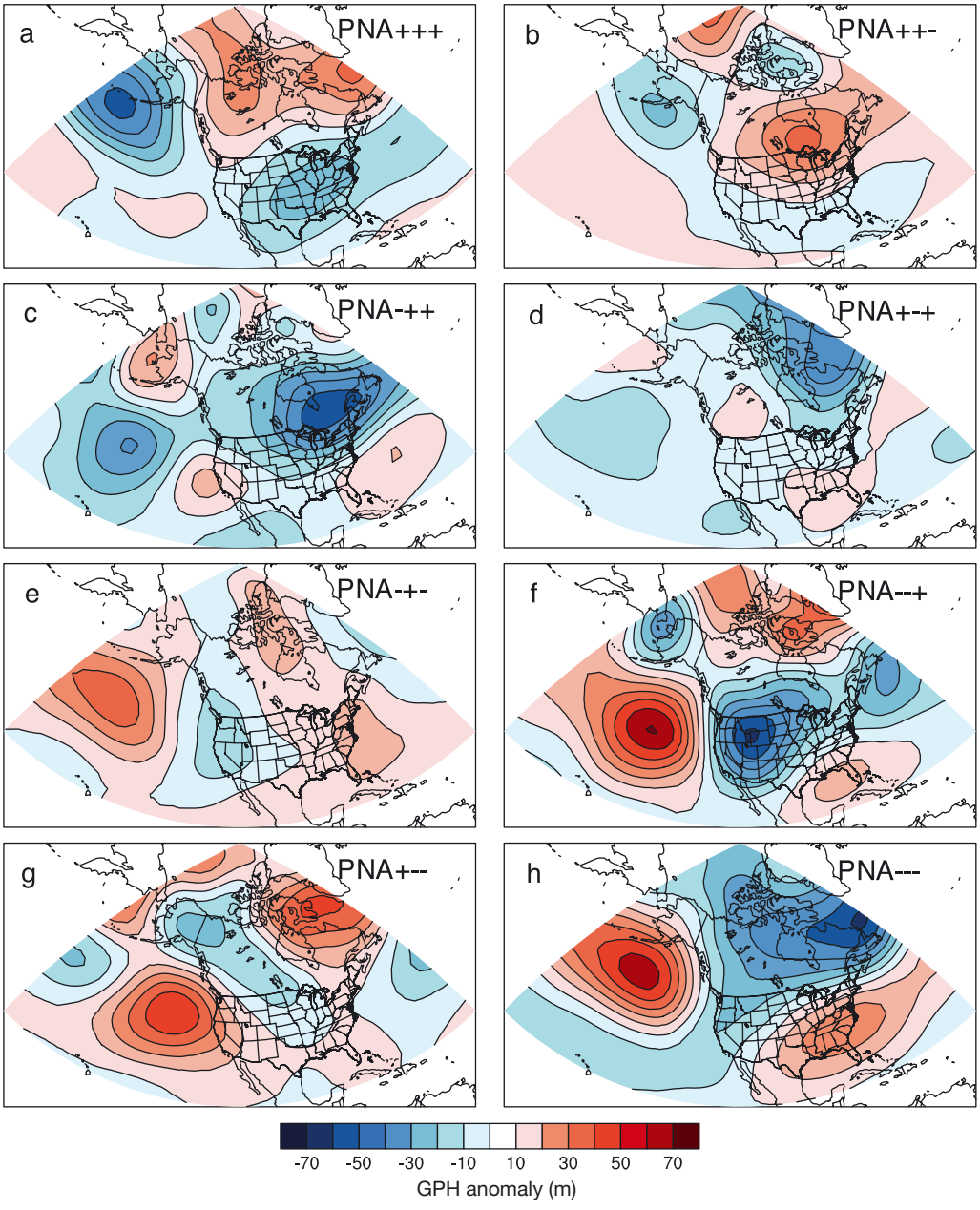

Fig. 7. Composite 500 hPa geopotential height (GPH) anomalies (from the 1981–2010 mean) by Pacific–North American (PNA) intraseasonal phase distribution as described in Table 5

regional-to-continental interactions between snow cover and atmospheric circulation in light of recent SST changes in the North Pacific Ocean, including abnormally warm northeastern Pacific waters observed during the winter of 2013–2014 (Bond et al. 2015) which overlapped a transition to positive PDO conditions known to influence the downstream NA snowpack (McCabe & Dettinger 2002). Continued assessments of ocean–atmosphere linkages to subcontinental snow properties are critical, as losses in transient snow cover amidst a changing climate increasingly affect water resources, especially over Western NA (Pederson et al. 2013, Mote et al. 2016).

Acknowledgements. The Editor and 3 anonymous reviewers are thanked for constructive comments that led to manuscript improvements. We also thank Daniel Steinhoff for computational guidance involving snow data processing. We used the Web-based Reanalysis Intercomparison Tool (https://www.esrl.noaa.gov/psd/cgi-bin/data/testdap/plot.comp.pl) to create Fig. S4.

LITERATURE CITED

Abatzoglou JT (2011) Influence of the PNA on declining mountain snowpack in the Western United States. Int J Climatol 31:1135–1142

Ballinger TJ, Sheridan SC (2016) Sea ice impacts on polar surface weather types in the North American Arctic. Clim Res 67:117–134

Ballinger TJ, Allen MJ, Rohli RV (2014) Spatiotemporal analysis of the January Northern Hemisphere circumpolar vortex over the contiguous United States. Geophys Res Lett 41:3602–3608

Barnston AG, Livezey RE (1987) Classification, seasonality and persistence of low-frequency atmospheric circulation patterns. Mon Weather Rev 115:1083–1126

Bednorz E (2004) Snow cover in eastern Europe in relation to temperature, precipitation and circulation. Int J Climatol 24:591–601

Bond NA, Cronin MF, Freeland H, Mantua N (2015) Causes and impacts of the 2014 warm anomaly in the NE Pacific. Geophys Res Lett 42:3414–3420

Brown RD (2000) Northern hemisphere snow cover variability and change, 1915–97. J Clim 13:2339–2355

Brown RD, Derksen C (2013) Is Eurasian October snow cover extent increasing? Environ Res Lett 8:024006

Brown RD, Robinson DA (2011) Northern Hemisphere spring snow cover variability and change over 1922–2010 including an assessment of uncertainty. Cryosphere 5:219–229

Brown RD, Brasnett B, Robinson D (2003) Gridded North American monthly snow depth and snow water equivalent for GCM validation. Atmos-Ocean 41:1–14

Brown RD, Derksen C, Wang LB (2010) A multi-data set analysis of variability and change in Arctic spring snow cover extent, 1967–2008. J Geophys Res Atmos 115: D16111

Bulygina ON, Razuvaev VN, Korshunova NN (2009) Changes in snow cover over Northern Eurasia in the last few decades. Environ Res Lett 4:045026

Cassano EN, Glisan JM, Cassano JJ, Gutowski WJ Jr, Seefeldt MW (2015) Self-organizing map analysis of widespread temperature extremes in Alaska and Canada. Clim Res 62:199–218

Cohen J, Ye H, Jones J (2015) Trends and variability in rain-on-snow events. Geophys Res Lett 42:7115–7122

Comiso JC, Hall DK (2014) Climate trends in the Arctic as observed from space. Wiley Interdiscip Rev Clim Change 5:389–409

Coumou D, Lehmann J, Beckmann J (2015) The weakening summer circulation in the North Hemisphere mid-latitudes. Science 348:324–327

Dai LY, Che T (2014) Spatiotemporal variability in snow cover from 1987 to 2011 in northern China. J Appl Remote Sens 8:084693

Derksen C, Brown R (2012) Spring snow cover extent reductions in the 2008–2012 period exceeding climate model projections. Geophys Res Lett 39:L19594

Derksen C, Brown R, Mudryk L, Luojus K (2016) Terrestrial snow cover. In: Arctic Report Card 2016. http://www.arctic.noaa.gov/Report-Card/Report-Card-2016/ArtMID/5022/ArticleID/276/Terrestrial-Snow-Cover

Estilow TW, Young AH, Robinson DA (2015) A long-term Northern Hemisphere snow cover extent data record for climate studies and monitoring. Earth Syst Sci Data 7: 137–142

Feldstein SB (2000) The timescale, power spectra, and climate noise properties of teleconnection patterns. J Clim 13:4430–4440

Foster J, Hall D, Robinson DA, Estilow T (2008) Spring snow melt timing and changes over Arctic lands. Polar Geogr 31:145–157

Foster JL, Cohen J, Robinson DA, Estilow TW (2013) A look at the date of snowmelt and correlations with the Arctic Oscillation. Ann Glaciol 54:196–204

Francis J, Skific N (2015) Evidence linking rapid Arctic warming to mid-latitude weather patterns. Philos Trans R Soc A 373:20140170

Francis JA, Vavrus SJ (2012) Evidence linking Arctic amplification to extreme weather in mid-latitudes. Geophys Res Lett 39:L06801

Francis JA, Vavrus SJ (2015) Evidence for a wavier jet stream in response to rapid Arctic warming. Environ Res Lett 10:014005

Frei A, Robinson DA (1999) Northern hemisphere snow extent: regional variability 1972–1994. Int J Climatol 19: 1535–1560

Frei A, Robinson DA, Hughes MG (1999) North American snow extent: 1900–1994. Int J Climatol 19:1517–1534

Frei A, Tedesco M, Lee S, Foster J, Hall DK, Kelly R, Robinson DA (2012) A review of global satellite-derived snow products. Adv Space Res 50:1007–1029

Ge Y, Gong G, Frei A (2009) Physical mechanisms linking the winter Pacific-North American teleconnection pattern to spring North American snow depth. J Clim 22: 5135–5148

Ghatak D, Frei A, Gong G, Stroeve J, Robinson D (2010a) On the emergence of an Arctic amplification signal in terrestrial Arctic snow extent. J Geophys Res Atmos 115: D24105

Ghatak D, Gong G, Frei A (2010b) North American temperature, snowfall, and snow-depth response to winter climate modes. J Clim 23:2320–2332

Hall R, Erdelyi R, Hanna E, Jones JM, Scaife AA (2015) Drivers of North Atlantic polar front jet stream variability. Int J Climatol 35:1697–1720

Hawkins TW, Ellis AW, Skindlov JA, Reigle D (2002) Intra-annual analysis of the North American snow cover-monsoon teleconnection: seasonal forecasting utility. J Clim 15:1743–1753

Henderson GR, Leathers DJ (2010) European snow cover variability and associations with atmospheric forcings. Int J Climatol 30:1440–145

Hernández-Henríquez MA, Déry SJ, Derksen C (2015) Polar amplification and elevation-dependence in trends of Northern Hemisphere snow cover extent, 1971–2014. Environ Res Lett 10:044010

Kalnay E, Kanamitsu M, Kistler R, Collins W and others (1996) The NCEP/NCAR 40-year reanalysis project. Bull Am Meteorol Soc 77:437–471

Kim Y, Kimball JS, Robinson DA, Derksen C (2015) New satellite climate data records indicate strong coupling between recent frozen season changes and snow cover over high northern latitudes. Environ Res Lett 10:084004

Kluver D, Leathers D (2015) Regionalization of snowfall frequency and trends over the contiguous United States. Int J Climatol 35:4348–4358

Kluver D, Mote T, Leathers D, Henderson GR, Chan WH, Robinson DA (2016) Creation and validation of a comprehensive 1° by 1° daily gridded North American dataset for 1900–2009: snowfall. J Atmos Ocean Technol 33:857–871

Knowles N (2015) Trends in snow cover and related quantities at weather stations in the conterminous United States. J Clim 28:7518–7528

Kunkel KE, Palecki MA, Hubbard KG, Robinson DA, Redmond KT, Easterling DR (2007) Trend identification in twentieth-century US snowfall: the challenges. J Atmos Ocean Technol 24:64–73

Kunkel KE, Palecki M, Ensor L, Hubbard KG, Robinson D, Redmond K, Easterling D (2009) Trends in twentieth-century U.S. snowfall using a quality-controlled dataset. J Atmos Ocean Technol 26:33–44

Kunkel KE, Robinson DA, Champion S, Yin X, Estilow T, Frankson RM (2016) Trends and extremes in Northern Hemisphere snow characteristics. Curr Clim Change Rep 2:65–73

Leathers DJ, Mote TL, Kuivinen KC, McFeeters S, Kluck DR (1993) Temporal characteristics of USA snowfall 1945–1946 through to 1984–1985. Int J Climatol 13:65–76

Leathers DJ, Mote TL, Grundstein AJ, Robinson DA, Felter K, Conrad K, Sedywitz L (2002) Associations between continental-scale snow cover anomalies and air mass frequencies across Eastern North America. Int J Climatol 22:1473–1494

McCabe GJ, Dettinger MD (2002) Primary modes and predictability of year-to-year snowpack variations in the western United States from teleconnections with Pacific Ocean climate. J Hydrometeorol 3:13–25

Mioduszewski JR, Rennermalm AK, Robinson DA, Wang L (2015) Controls on spatial and temporal variability in the Northern Hemisphere terrestrial snow melt timing, 1979–2012. J Clim 28:2136–2153

Mote PW, Rupp DE, Li S, Sharp DJ and others (2016) Perspectives on the causes of exceptionally low 2015 snowpack in the western United States. Geophys Res Lett 43: 10980–10988

Najafi MR, Zwiers FW, Gillett NP (2016) Attribution of the spring snow cover extent decline in the Northern Hemisphere, Eurasia, and North America to anthropogenic influence. Clim Change 136:571–586

Overland JE (2016) A difficult Arctic science issues: midlatitude weather linkages. Polar Sci 10:210–216

Overland JE, Dethloff K, Francis JA, Hall RJ and others (2016) Nonlinear response of mid-latitude weather to the changing Arctic. Nat Clim Chang 6:992–998

Pederson GT, Betancourt JL, McCabe GJ (2013) Regional patterns and proximal causes of the recent snowpack decline in the Rocky Mountains, U.S. Geophys Res Lett 40:1811–1816.

Peng S, Piao S, Ciais P, Friedlingstein P, Zhou LM, Wang T (2013) Change in snow phenology and its potential feedback to temperature in the Northern Hemisphere over the last three decades. Environ Res Lett 8:014008

Pohl S, Marsh P, Liston GE (2006) Spatial-temporal variability in turbulent fluxes during spring snowmelt. Arc Antarct Alp Res 38:136–146

Robinson DA (1989) Evaluation of the collection, archiving and publication of daily snow data in the United States. Phys Geogr 10:120–130

Robinson DA, Frei A (2000) Seasonal variability of northern hemisphere snow extent using visible satellite data. Prof Geogr 52:307–315,

Robinson DA, Kukla G (1988) Comments on 'Comparison of Northern Hemisphere snow cover data sets'. J Clim 1: 435–440,

Robinson DA, Dewey KF, Heim RR Jr (1993) Global snow cover monitoring — an update. Bull Am Meteorol Soc 74: 1689–1696

Robinson DA, Estilow TW, NOAA CDR Program (2012) NOAA Climate Data Record (CDR) of Northern Hemisphere (NH) Snow Cover Extent (SCE), Version 1. NOAA National Centers for Environmental Information. https://data.nodc.noaa.gov/cgi-bin/iso?id=gov.noaa.ncdc:C00756

Ross B, Walsh JE (1986) Synoptic-scale influences of snow cover and sea ice. Mon Weather Rev 114:1795–1810

Rupp DE, Mote PW, Bindoff NL, Stott PA, Robinson DA (2013) Detection and attribution of observed changes in Northern Hemisphere spring snow cover. J Clim 26: 6904–6914

Serreze MC, Clark MP, McGinnis DL, Robinson DA (1998) Characteristics of snowfall over the eastern half of the United States and relationships with principal modes of low-frequency atmospheric variability. J Clim 11:234–250

Tang Q, Zhang X, Francis JA (2014) Extreme summer weather in northern mid-latitude linked to a vanishing cryosphere. Nat Clim Chang 4:45–50

Thackeray CW, Fletcher CG (2016) Snow albedo feedback: current knowledge, importance, outstanding issues and future directions. Prog Phys Geogr 40:392–408

Vavrus SJ, Wang F, Martin JE, Francis JA, Peings Y, Cattiaux J (2017) Changes in North American atmospheric circulation and extreme weather: influence of Arctic amplification and Northern Hemisphere snow cover. J Clim 30:4317–4333

Vega AJ, Henderson KG, Rohli RV (1995) Comparison of monthly and intramonthly indices for the Pacific-North American teleconnection pattern. J Clim 8:2097–2103

Walsh JE, Tucek DR, Peterson MR (1982) Seasonal snow cover and short-term fluctuations over the United States. Mon Weather Rev 110:1474–1485

Wang T, Pang S, Ottle C, Ciais P (2015) Spring snow cover deficit controlled by intraseasonal variability of the surface energy fluxes. Environ Res Lett 10:024018

Editorial responsibility: Gerrit Hoogenboom, Gainesville, Florida, USA

Submitted: February 20, 2017; Accepted: November 2, 2017
Proofs received from author(s): January 17, 2018